Hindawi
Advances in Civil Engineering
Volume 2021, Article ID 8819015, 14 pages
https://doi.org/10.1155/2021/8819015

Research Article

Shear Strength Behavior of Sand Reinforced by Kraft Paper Using the Ring Shear Apparatus

Wan-li Xie,[1,2] **Qianyi Guo**,[3] **Nelson N.S. Chou**,[1] **Rongsen Zhu**,[1] **and Maosheng Zhang**[1,2]

[1]*State Key Laboratory of Continental Dynamics, Department of Geology, Northwest University, Xi'an, Shaanxi 710069, China*
[2]*Key Laboratory for Geo-Hazards in Loess Area, Ministry of Land and Resources, Xi'an Center of China Geological Survey, Xi'an, Shaanxi 710054, China*
[3]*Shaanxi Hydraulic Environment Investigation Center, Xi'an, Shaanxi 710069, China*

Correspondence should be addressed to Wan-li Xie; xiewanli@nwu.edu.cn

Received 2 September 2020; Revised 15 October 2020; Accepted 3 September 2021; Published 29 October 2021

Academic Editor: Jian Xu

To explore the reinforcement effects of different reinforcement methods, kraft paper was used as reinforcement material, and shear tests were carried out in sand to study the reinforcement effects of kraft paper perpendicular and parallel to the shear plane. The test results show that the two reinforcement methods can effectively improve the strength of sand and the orthogonal reinforcement form is more superior. The existence of reinforced materials greatly improves the cohesion of sand, but does not significantly improve the internal friction angle. The width of reinforcement material has little effect on the reinforcement effect and shows different variation laws under different reinforcement forms.

1. Introduction

Owing to the advantages of easy construction, cost effectiveness, environmental friendliness, and excellent seismic performance compared with traditional materials, geosynthetics are widely used in construction engineering [1–8]. With the development of geosynthetics technology, an increasing number of new materials are being used [9–12], with satisfactory results. In recent years, reinforcement technology has been widely used in construction in China. Reinforced structures such as reinforced retaining walls and reinforced subgrades effectively improve the tensile and shear strength of the earth fill and reduce the engineering cost to some extent. In collapsible loess or cohesive force sandy soil areas, reinforcement materials enhance the overall construction stability. Research on reinforcement materials, reinforced soil, and reinforcement methods has been advancing rapidly.

The interaction between reinforcement material and soil is complex due to the diversity of physical and mechanical properties [13, 14]. To some extent, the interaction affects the strength and deformation characteristics of reinforced soil. Research on strength deformation characteristics of reinforced soil traditionally uses a three-axis test [15–17]. In [18], horizontal and vertical three-axis shear tests were conducted on unconsolidated reinforced saturated sand and its strength characteristics and failure modes were studied. The results showed that the shear strength of the reinforced sand increased significantly. In [19], the shear strength of reinforced soil under different reinforcement conditions was studied through three-axis UU shear tests. The results showed that reinforcement effectively increased cohesion, but had little effect on the internal friction angle. In [20], three-axis creep tests were conducted on plain soil and reinforced soil with different confining pressures and reinforced layers to explore the long-term degeneration characteristics of reinforced soil and the reinforcement mechanism involved. To study the strength deformation characteristics of coarse-grained soil and reinforced coarse-grained soil, three-axis shear tests were conducted in [21, 22]. In [23], a GDS dynamic three-axis system was used to study the deformation characteristics of reinforced loess under different dynamic loads. The results showed that the antivibration performance of soil is improved with an increase in the number of reinforced

layers. Tests have been conducted to explore the interaction between geosynthetics and soil [24–29], [30] and mathematical models have been proposed [31–37]. Although model tests can help in understanding the dynamic response characteristics of reinforced soil, numerical simulation results are more intuitive [38–46]. In [47], [48], [49, 50], and [51], the two-dimensional barrier was broken to conduct three-dimensional discrete element analysis. Numerical analysis has been regarded as an effective and convenient means of studying the behavior of different types of structures under self-weight and loading conditions in geotechnical engineering.

Under external load, the interaction between the reinforcement material and soil is reflected in the frictional resistance produced by their surfaces coming into contact. The mechanical properties of the soil are changed, and the deformation characteristics of the reinforced soil are influenced. Moreover, different methods of reinforcement, stress level, and stress-strain state greatly influence the interaction between the reinforcement material and the soil; the stress-strain relationship becomes complex, which further affects the shear strength of the reinforced soil. Thus, accurate determination and selection of the shear strength parameters of reinforcement materials must be considered during the construction process [52]. The ring shear apparatus has a uniform stress distribution owing to its special structure. It has certain advantages when analyzing the stress, strain, and shear strength properties of each contact surface under large displacement. In [53–55], the interfacial shear properties of different reinforcement materials and different soils were studied using the ring shear test and the differences in shear strength of different reinforcement materials were verified. To explore the dynamic response characteristics of reinforced sand, a series of load tests, tensile tests, and shear tests have been conducted. The results showed that different reinforcement and test methods have different effects on the strength of reinforced sand [56–59]. Currently, there are few studies on using kraft paper to increase the strength of sand. In [60], kraft paper was added in sand and clay at 5%, 10%, and 15% of dry soil mass. The results show that the content and humidity have significant effects on the improvement of soil strength. Fiber makes the soil ductile and can maintain the shear strength at high strain level. However, further research is necessary due to the complexity of the mechanical behavior of reinforced sand.

On the basis of previous studies, the shear strength of the sand reinforced with kraft paper was measured by using the ring shear apparatus. To explore the reinforcement effect of different reinforcement methods, kraft paper was used as the sand reinforcement material to study the stress-strain relationship and residual strength characteristics of the reinforced soil under large displacements. Controlling the relative density of the sand, the ring shear tests were conducted to assess the strength and deformation characteristics of kraft-reinforced sandy soil with different widths and different reinforcing methods (parallel shear planes and vertical shear planes). Different widths, two reinforcement methods under different external load stress and strain characteristics, and variations in the shear strength were used to explore the reinforcement effects on the strength of the reinforced soil.

2. Test Materials, Instruments, and Schemes

2.1. Test Materials. Dry and clean medium coarse sand was selected for the experiments. The particle size was concentrated from 0.5–2.0 mm. The grain gradation curve is shown in Figure 1. The maximum dry density and minimum dry density of the sand used in the test were 2.26 g/cm^3 and 1.62 g/cm^3, respectively.

The reinforcement material used in the test was kraft paper meeting the 100 g specification of the nonstripe envelopes specified. The kraft paper is flexible, strong, environmentally friendly, and durable as a food packaging material. It has some antiwet deformation ability and can withstand low temperature as well as thermal expansion and contraction; these properties prevent its deformation, distortion, and wrinkling. Kraft paper made of wood fiber and resin binder has high tensile strength, rupture strength, and dynamic power. The tensile strength of the kraft paper per unit width measured by using a digital material testing machine was 80 N/cm, with the strain of 0.67 at failure.

2.2. Test Instrument. Ring shear apparatus plays an important role in the research of the landslide disaster mechanism [61–63]. The ring shear apparatus used in this test was a dynamic ring shear apparatus of SRS-150 unsaturated soil produced by GCTS Testing Systems in the United States. The inner ring diameter of the shear box was 100 mm, outer ring diameter was 150 mm, effective height was 25 mm, shear area was 98 cm^2, shear plane was constant, and shear displacement was continuously maintained. The ring shear apparatus can be used to determine the shear strength and residual strength parameters under large displacements. The maximum axial pressure of the ring shear device was 10 kN, and the shear rate range was 0.001–1 rev/min. The operating principle of the ring shear instrument is shown in Figure 2.

2.3. Test Scheme. In this experiment, the ring shear instrument was used to study the reinforcement effect of kraft paper as the reinforcement material for a sand-retaining wall. Different from the linear failure formed by the unreinforced sand-retaining wall, the failure surface of the reinforced sand-retaining wall is an approximate circular shear surface, as shown in Figure 3. At the top of the slope, the reinforced material is in orthogonal contact with the failure surface, and at the bottom of the slope, the reinforced material is in nearly parallel contact with the failure surface. Therefore, two reinforcement forms of kraft paper and shear plane are designed, which are orthogonal and parallel. The reinforcement of the sample is shown in Figure 4. The experiment takes two forms of reinforcement and carries out the four widths of kraft paper under four vertical stresses. A total of 32 sets of tests are carried out (Table 1).

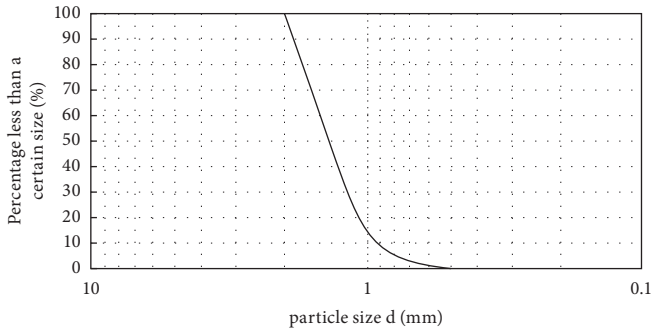

Figure 1: Grain size distribution curve of sand used in tests.

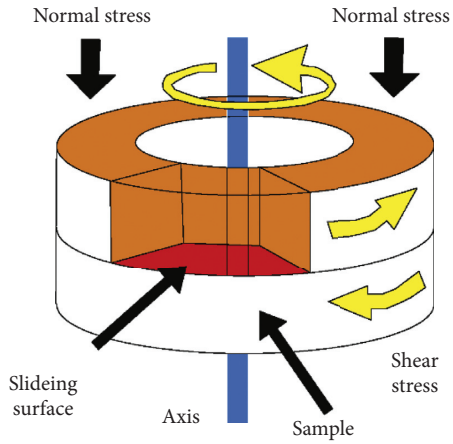

Figure 2: Schematic diagram of ring shear process.

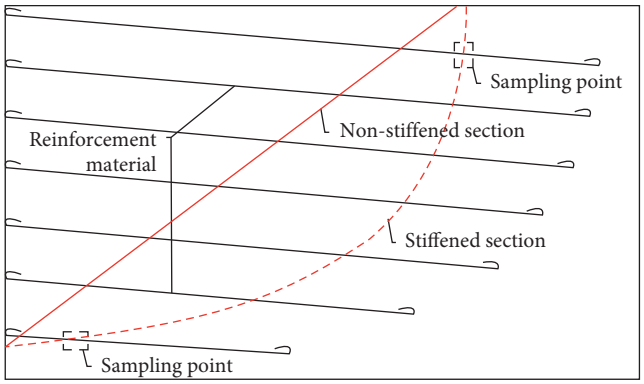

Figure 3: Diagram of the failure plane of reinforced walls.

3. Test Results and Analysis

3.1. Analysis of Stress-Strain Characteristics. According to the test scheme, the ring shear test was conducted on the vertical pressure of the reinforced sand and the non-reinforced sand under conditions of 15 kPa, 30 kPa, 40 kPa, and 50 kPa. The relationship between the shear stress and shear displacement of nonreinforced sand under different pressure conditions is shown in Figure 5. Under different vertical pressures, the shear time is a constant concussion of the wrong curve. The shear stress-shear displacement curve [64] for cohesive soils such as loess is very different; the sand particles differ in size, and the cohesive force is almost zero. When the constant vertical pressure is subjected to torsion shear, the reciprocal extrusion between the particles on the shear surface is turned over and friction dislocation occurs. The shear strength of the sand is in the range of the lower boundary of the shear stress-shear displacement curve. In this study, the shear strength of the sand is defined by the peak point of the upper boundary curve.

As shown in Figure 5, under different vertical pressures, the shear deformation of nonreinforced sandy soil is fast; the shear stress reaches the peak value. A brief strain softening occurs later, and the shear force decreases. With an increase in shear displacement, shear stress continues to increase in the later stage, which is characterized by strain hardening. The hardening property is more obvious when the vertical pressure is low; the vertical constraint during sand shear is smaller between particles over the required resistance, dislocation, and flip. The dilatancy effect between particles is relatively obvious in the shear process of the nonreinforced sand. The compression displacementshear displacement curve is shown in Figure 6. Compared with the trend of the holistic shear shrinkage stress under a vertical pressure of 50 kPa, when the vertical pressure is 15 kPa and 30 kPa, the compression curves indicate dilatancy, shear contraction, and an oscillatory trend. Thus, to overcome the sand friction, dislocation resistance, and dilatancy, the sand is turned over and cut. Under a low vertical pressure, the shear stress increases with an increase in shear displacement. When the shear stress reaches the second peak with an increase in shear displacement, the nonreinforced sand enters the strain-softening region.

The shear stress-shear displacement curves for two reinforcement methods under different vertical pressures and with different reinforcement material widths are shown in Figures 7–14.

The shear stress-shear displacement curve of the reinforced soil is the same as that of the nonreinforced sandy soil. The shear stressshear displacement curve of kraft paper-reinforced sand is also a shock dislocation curve. In the shear stress-shear displacement curve of kraft paper-reinforced sand with a vertical pressure of 50 kPa and a kraft paper width between 0.2 cm and 0.6 cm, the region of peak shear strength is reached. The vibration characteristic curve of shear stress in the 6–8 mm region of shear displacement is shown in Figure 15. The shear stress vibration amplitude of the vertical-reinforced sand is larger than that of the horizontal-reinforced sand and the nonreinforced sand, indicating that vertical reinforcement is a spatial constraint in the process of sand friction reversal that effectively increases the frictional resistance between sand particles and promotes the "enhancement effect" of shear stress in the process of sand particle turning.

This pattern of reinforcement is parallel to the horizontal ring fabric of a shear plane due to a reduced friction fault on the shear plane under the soil particles. The contact surface between the kraft paper and sand particles is smoother; the shear stress-shear displacement curve of the relative volatility is smaller compared with the vertical-reinforced sand, especially at 0.6 cm. The horizontal annular kraft paper-

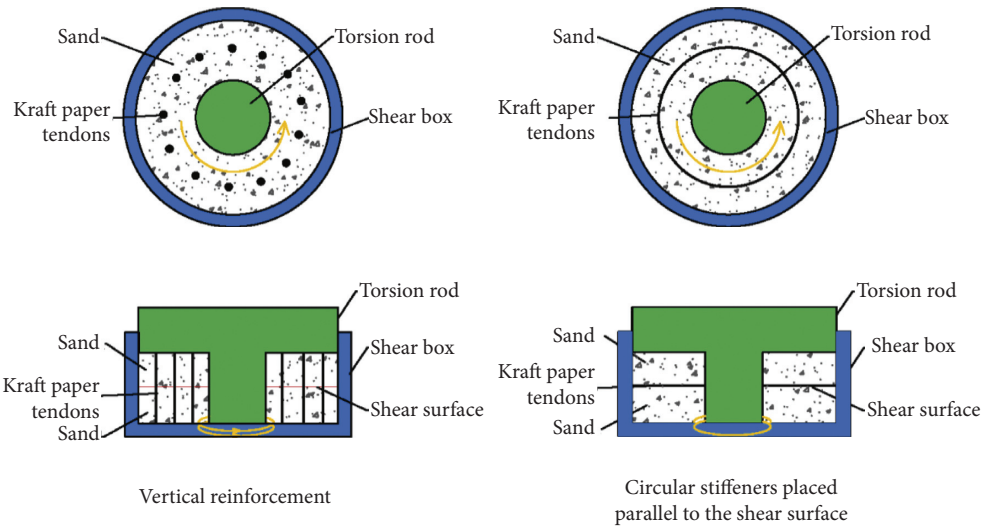

Figure 4: Diagram of directions and test methods of reinforcements in ring shear tests.

Table 1: Test conditions.

Vertical pressures (kPa)	Reinforcement material widths (cm)	Reinforcement forms
15	0.2	Parallel to the shear plane
30	0.4	
40	0.6	Perpendicular to the shear plane
50	0.8	

reinforced sand shear stress-shear displacement curves for the shear stress range of shocks are much less than those for the nonreinforced sand shear stress range of shocks.

Comparing Figures 5, 8, 10, 12, and 14, it can be seen that (1) the characteristics of the softened area of the vertical-reinforced sand are not obviously different from those of the nonreinforced sand. The shear stress and shear displacement curves enter the strain-hardening area after shear initiation. (2) The strain-hardening characteristics of vertical kraft-reinforced sand are more obvious than those of nonreinforced sand. Under higher pressure, vertical reinforcement can help sand continuously resist greater shear stress during shearing.

Comparing Figures 5, 7, 9, 11, and 13, it can be seen that (1) the early strain-softening characteristics of horizontal-reinforced sandy soil parallel to the shear plane are different from those at different vertical pressures. At high pressure, the early strain-softening characteristics are less than those of nonreinforced sand. Under the restraining effect of 40 kPa and 50 kPa, the reinforcement effect is evident at the beginning of shear, and the frictional resistance of the sand particles on the shear surface continuously increases. (2) The shear stress-shear displacement curve strain-hardening characteristic of horizontal-reinforced sand is influenced by the width of the reinforcement material. When 0.6 cm kraft paper is used as the reinforcement material, the strain-hardening characteristics of the shear stress-shear displacement curve are lower than those of nonreinforced sand, due to the reduction in the friction force of the sand particles from placing the reinforcement material parallel to the shear surface. When the vertical pressure is relatively high, the strain-hardening phenomenon is more obvious when narrow vertical kraft paper is used as the reinforcement material. When the vertical pressure is relatively high, the strain-hardening characteristics decrease, and overall stiffness is observed. When a relatively narrow reinforcement material is placed parallel to the shear plane, the frictional resistance between the sand particles and the reinforcement material can be enhanced to some extent by higher pressure.

From the analysis, the shear strength of the nonreinforced sand is defined as the first peak point in the strain-softening zone. The shear strength of the vertical-reinforced sand and the horizontal-reinforced sand is defined as the peak point of the strain-hardening zone.

3.2. Analysis of Strength Characteristics of Sands Reinforced by Kraft Paper. Figure 16 shows the shear strength curve of vertical kraft paper-reinforced sand with different widths. The shear strength curve of vertical-reinforced sand is higher than that of nonreinforced sand, indicating that the vertical reinforcement method enhances the shear strength of sand. However, the effect of reinforcement on the shear strength of sand is more obvious under low pressure; 0.2 cm stiffened kraft paper exhibits the best effect. The shear strength is higher under different vertical pressures; when the 0.8 cm kraft paper is used as the reinforcing material, the reinforcement effect is most stable under different vertical pressures. The difference between the shear strength and the nonreinforced sand shear strength (approximately 11 kPa) is generally stable with increasing vertical pressure. Moreover, except for the optimum bar width of 0.2 cm, the

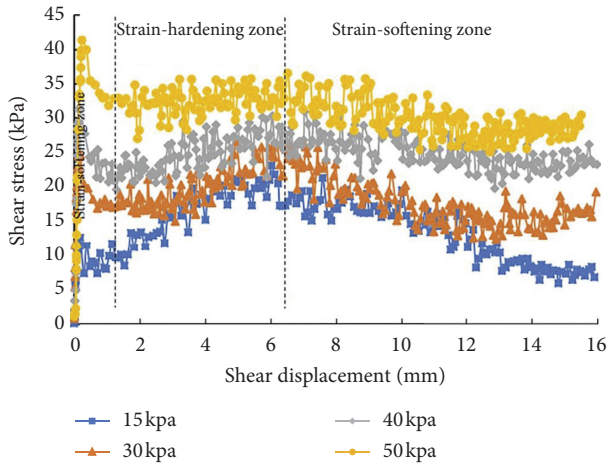

Figure 5: Shear stress and shear displacement curves of sand specimens.

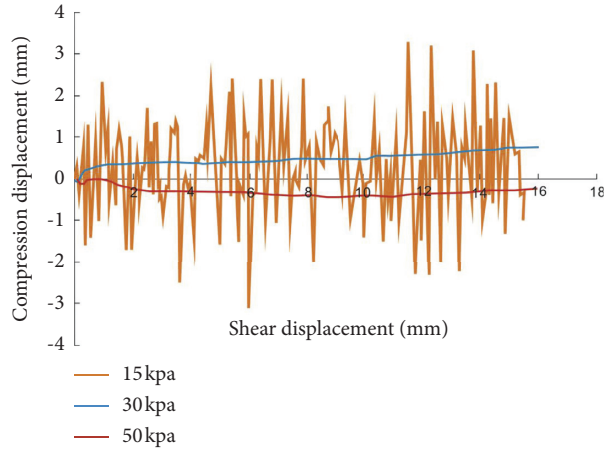

Figure 6: Relationship between compression displacement and shear displacement in nonreinforced sand in the shear process.

reinforcement effect on shear strength increases with width (for widths of 0.4 cm, 0.6 cm, and 0.8 cm), as shown in Figure 12.

Figure 17 shows the fitting curve of the shear strength and the vertical pressure of the horizontal annular kraft paper with different widths. When the kraft paper is placed in a ring parallel to the shear surface, the shear strength of sand is enhanced to some extent. The kraft paper with 0.4 cm width is the best for enhancing the shear strength of sand. The shear strength is greatest under vertical pressure. The reinforcement effect of 0.2 cm width kraft-reinforced sand is more stable. The shear strength of the kraft-reinforced sand under different vertical pressures is essentially the same as that of the nonreinforced sand (approximately 9 kPa). When the kraft paper is parallel to the shear plane, except for the optimum 0.4 cm bar width, the reinforcement effect on the shear strength (with bar widths of 0.2 cm, 0.6 cm, and 0.8 cm) is more obvious with decreasing kraft paper width.

To evaluate the influence of different reinforcement widths and reinforcement methods on the shear strength of sands, the reinforcement effect of the kraft paper on the shear strength of sand is evaluated. C is the cohesiveness of the nonreinforced sand, Cr is the cohesive force of the reinforced sand, φ is the internal friction angle of the nonreinforced sand, and φr is the internal friction angle of the reinforced sand. The cohesion growth rate of the reinforced sand is defined as $\varepsilon c = (cr - c)/c$, and the relative error rate of the internal friction angle of the reinforced sand is $\varphi r = (\varphi r - \varphi)/\varphi$, as shown in Table 2. Figures 14 and 15 show the relation curves of the cohesive force and the internal friction angle with the reinforcement width of the reinforced sand for the two reinforcement methods. From Table 2, we know that, in this test pressure range, using kraft paper as the reinforcement material can significantly enhance the cohesive force of sand; its cohesive force growth rate reaches 2025%–4950%, which has some effect on the internal friction angle. The relative error range of the internal friction angle is −16.2%–−5.41%.

From Table 2 and Figure 18, we can see that (1) the cohesive force of the reinforced sand with 0.2 cm width is greatest when perpendicular to the vertical reinforcement of the shear surface. At this time, the cohesion growth rate reaches 4950%. When the width of the bar was 0.4 cm, the cohesive force of the reinforced soil was the lowest; in the later stage, the cohesion showed a

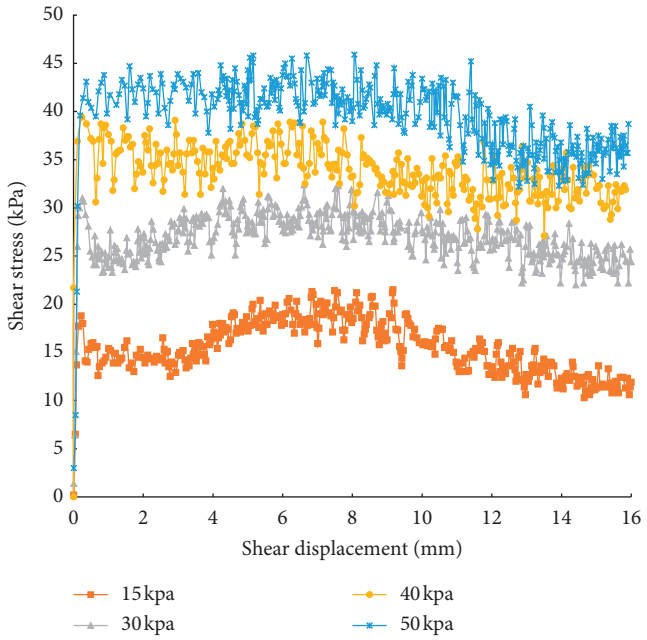

Figure 7: Shear stress-shear displacement curve of 0.6 cm horizontal ring-shaped-reinforced sand.

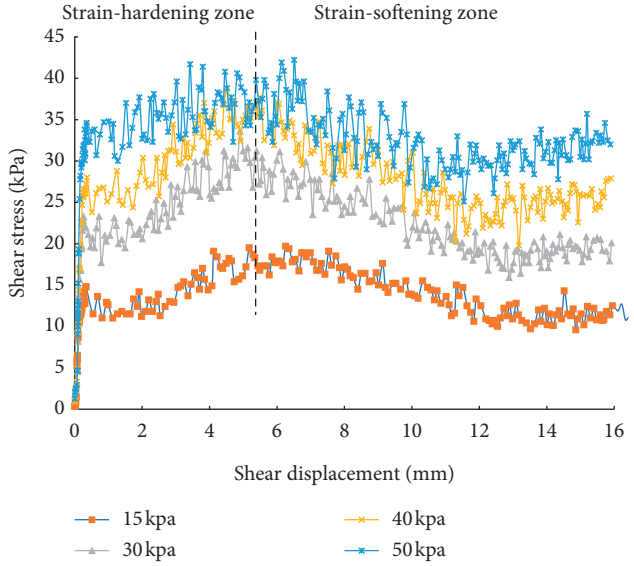

Figure 8: Shear stress-shear displacement curve of 0.6 cm vertical kraft paper-reinforced sand.

gradual increasing trend with increasing reinforcement width. (2) When placed in parallel, reinforced soil cohesion increases with an increase in reinforcement width from 0 cm to 0.4 cm. The maximum cohesion occurs when the reinforcement width is 0.4 cm; the cohesive strength growth rate is 4250%. (3) The cohesion growth rate of the vertical reinforcement is higher than that of the horizontal ring reinforcement under equal reinforcement width. Under the optimal reinforcement condition, the cohesion growth rate of the vertical reinforcement is higher than that of the horizontal ring reinforcement, indicating that vertical reinforcement is more effective than horizontal ring reinforcement in improving the cohesive force of sand.

From Table 2 and Figure 19, we can see that although the internal friction angle is less influenced by the width of the reinforcement material, the change trend is different with different reinforcement methods. When the kraft paper is parallel to the shear surface, the internal friction angle decreases with decreasing reinforcement width. When the kraft paper is perpendicular to the shear plane of the vertical reinforcement and the reinforcement is 0.2 cm–0.8 cm, the internal friction angle increases with increasing reinforcement width, indicating that, with reinforcement parallel to the horizontal shear plane ring, the friction between the sand particles continuously decreases with increasing width in this test pressure range.

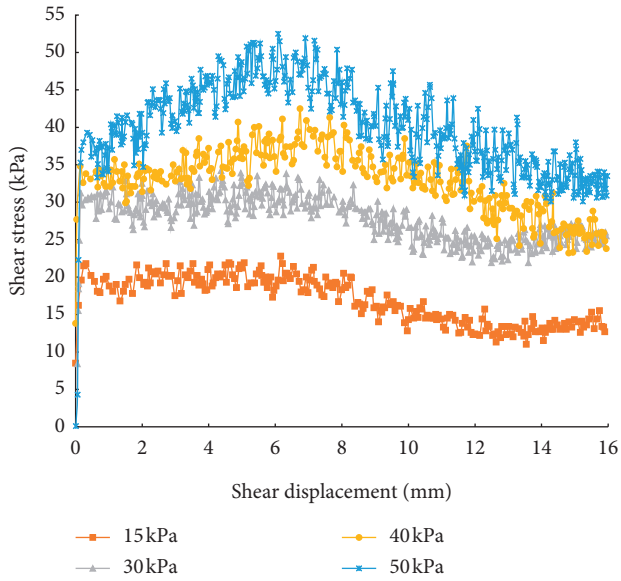

Figure 9: Shear stress-shear displacement curve of 0.2 cm horizontal ring-shaped-reinforced sand.

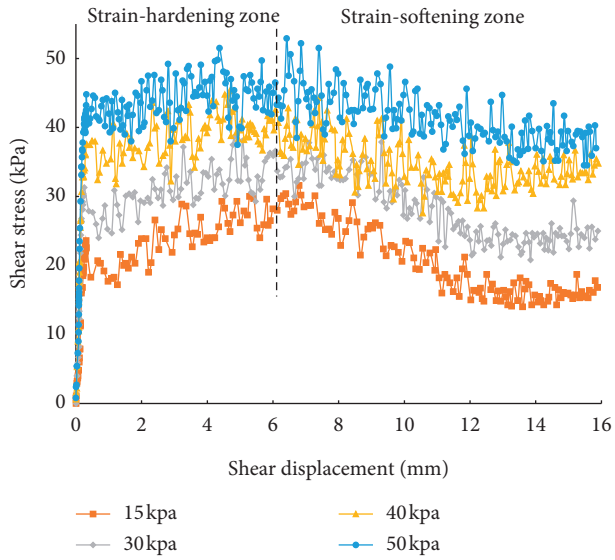

Figure 10: Shear stress-shear displacement curve of 0.2 cm vertical kraft paper-reinforced sand.

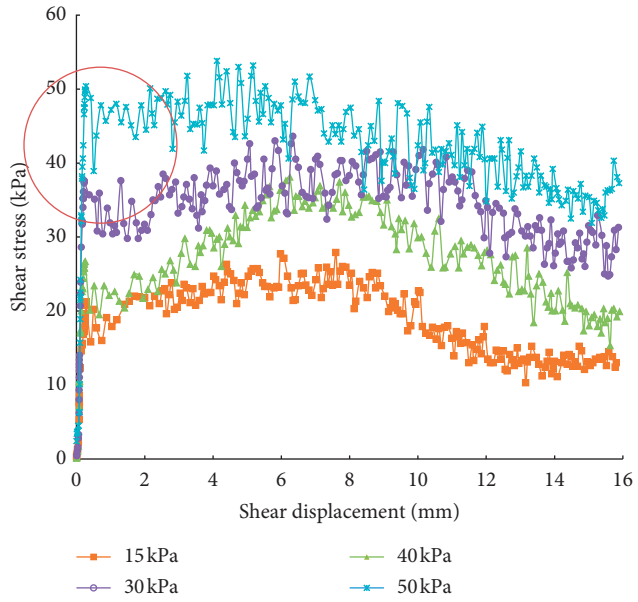

Figure 11: Shear stress-shear displacement curve of 0.4 cm horizontal ring-shaped-reinforced sand.

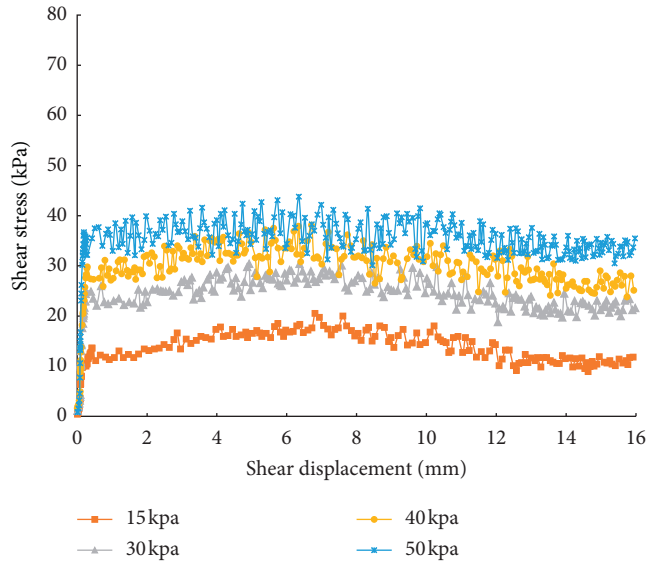

Figure 12: Shear stress-shear displacement curve of 0.4 cm vertical kraft paper-reinforced sand.

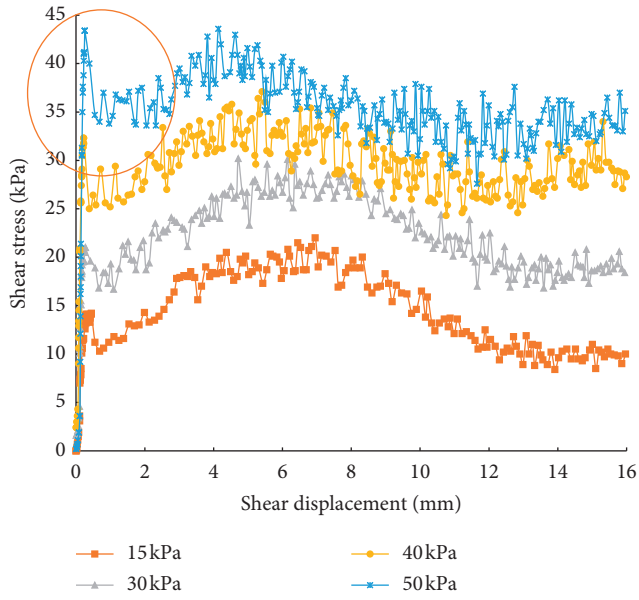

Figure 13: Shear stress-shear displacement curve of 0.8 cm horizontal ring-shaped-reinforced sand.

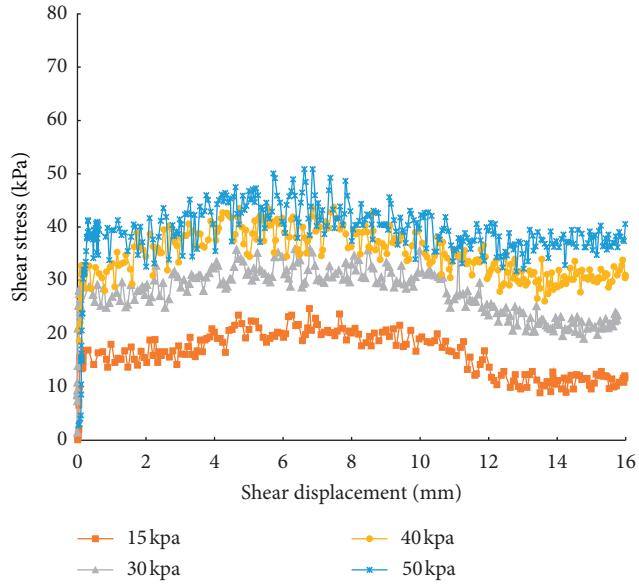

Figure 14: Shear stress-shear displacement curve of 0.8 cm vertical kraft paper-reinforced sand.

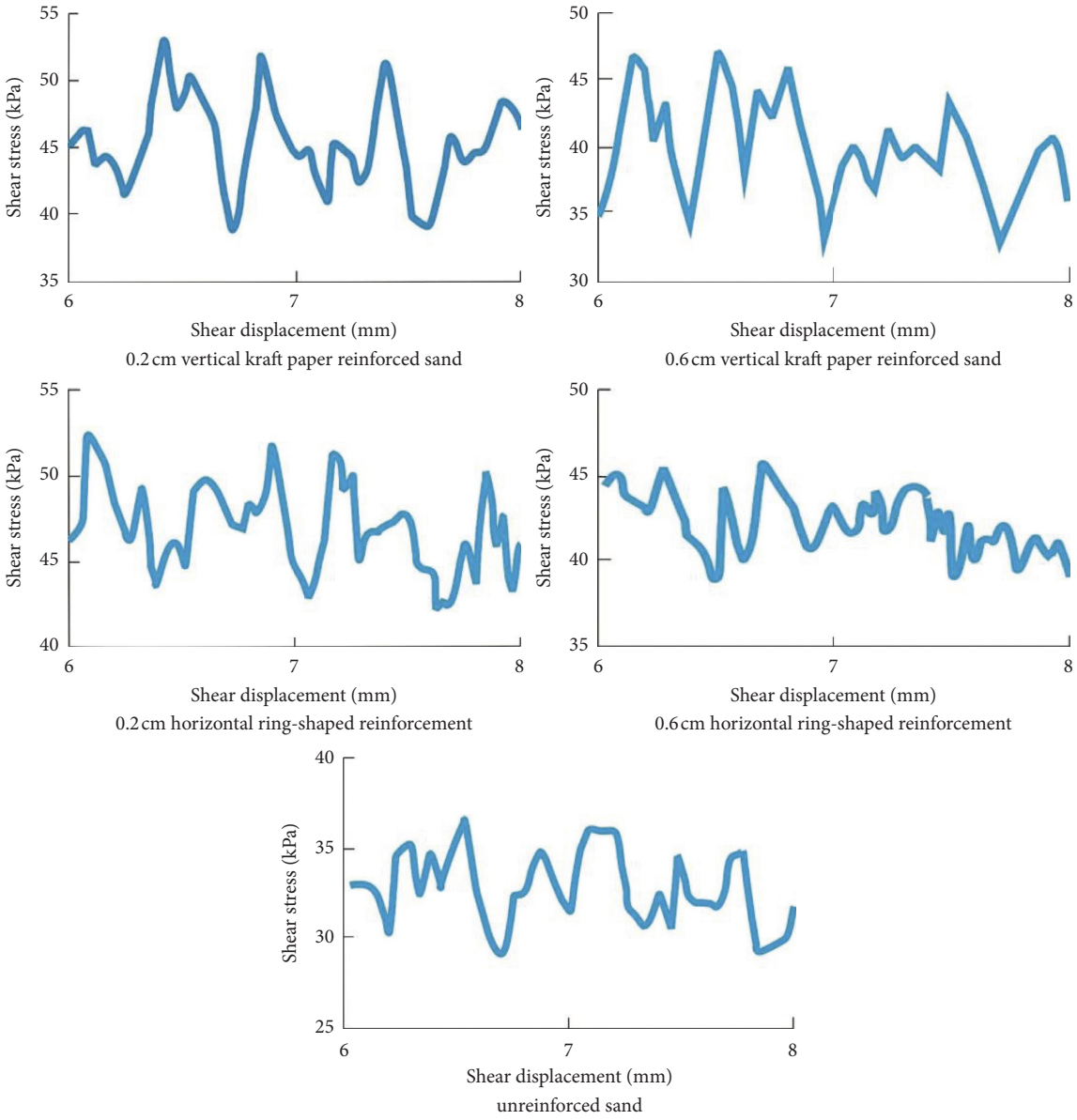

Figure 15: Vibration characteristics of shear stress in the 6–8 pfs region of shear displacement.

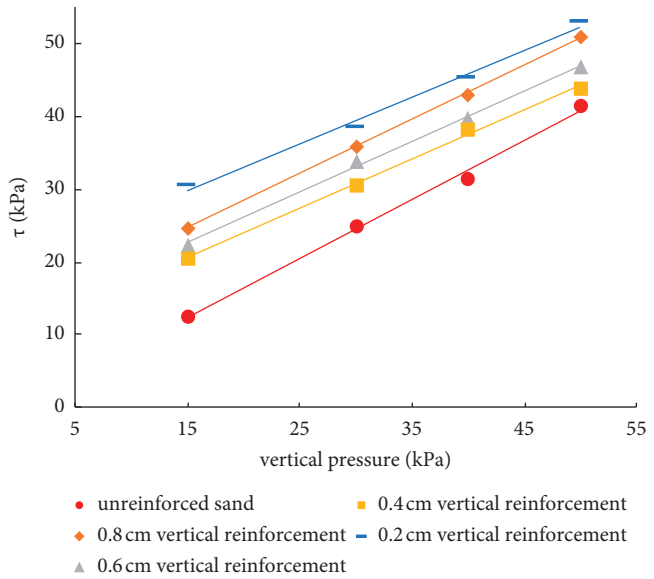

Figure 16: Shear strength curves of vertical-reinforced kraft paper with different widths.

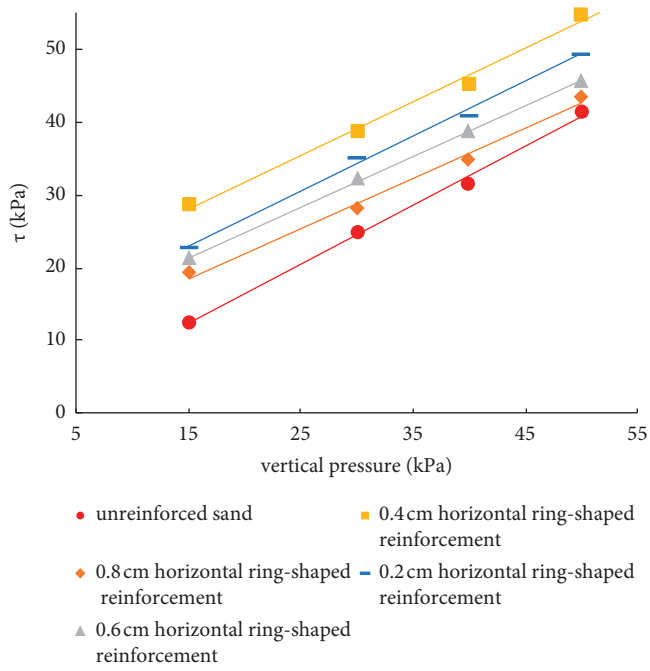

Figure 17: Shear strength curve of annular kraft paper-reinforced sand with different widths.

Table 2: Comparison of shear strength indexes.

Reinforcement category	Material parameter				
	Reinforcement width (cm)	C (kPa)	ε_c (%)	φ (°)	φ_r (%)
Nonreinforced sand	0	0.4	0	38.9	0
Vertical reinforcement	0.2	20.2	4950	32.6	−16.20
	0.4	10.4	2500	34.0	−12.60
	0.6	12.2	2950	34.9	−10.28
	0.8	13.5	3275	36.6	−5.91
Horizontal ring-shaped reinforcement	0.2	11.8	2850	36.9	−5.14
	0.4	17.4	4250	36.4	−6.43
	0.6	11.0	2650	34.9	−10.28
	0.8	8.5	2025	34.3	−11.83

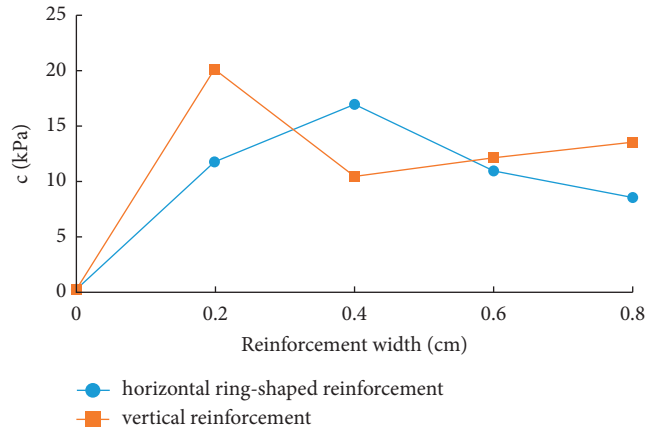

Figure 18: Relationship curves of the cohesive strength of reinforced sand and reinforcement width.

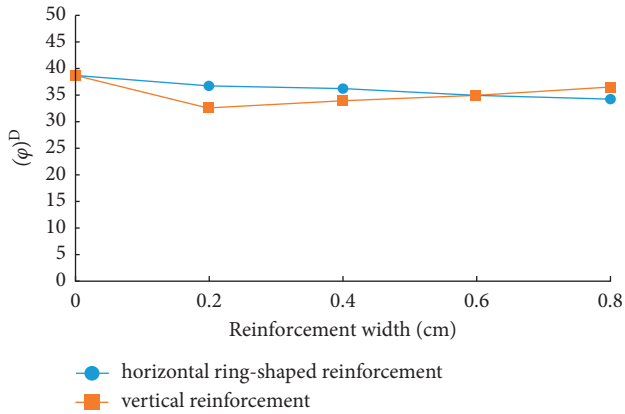

Figure 19: Relationship curves of the internal friction angle and the reinforcement width of reinforced sand.

4. Conclusions

In this paper, a comprehensive set of ring shear tests were carried out on samples of sand reinforced with parallel and vertical elements. The following conclusions are drawn from the results:

(1) The nonreinforced sand in the ring shear process curves of shear stress-shear displacement exhibits a shock slip curve; the increase in the shear displacement curve is divided into strain-softening and strain-hardening zones. Strain-softening and strain-hardening characteristics decrease with vertical stress. The curve enters the strain-hardening area after shear start up, and the strain-hardening property is enhanced compared with nonreinforced soil.

(2) The amplitude of the shear stress-shear displacement curve for kraft paper-reinforced sand is different for different reinforcement methods. The amplitude for reinforced sand with vertical reinforcement on the shear plane is significantly larger than for horizontal-ring-reinforced sand.

(3) The two reinforcement methods enhance the shear strength of sand. However, the optimum width of the horizontal shaft parallel to the shear plane was 0.4 cm; the optimum width of the vertical bar perpendicular to the shear plane was 0.2 cm.

(4) In this test pressure range, using kraft paper as the reinforcement material significantly enhances the cohesive force of sand; the internal friction angle has little influence on the width of the bar, and the trend of the change is different with different reinforcement methods.

Data Availability

Research data can be obtained from the corresponding author at any time.

Conflicts of Interest

The authors declare no conflicts of interest regarding the publication of this paper.

Acknowledgments

This study was financially supported by funding from the National Natural Science Foundation of China (41972292 and 41772323), the International Key Scientific and Technological Cooperation and Exchange Program in Shaanxi Province, China (2019KW-02), the National Key Research and Development Program of China (2017YFD0800501), and the Geological Survey Project of China Geological Survey (Grant no. DD20189270).

References

[1] R. Bhowmik, J. T. Shahu, and M. Datta, "Failure analysis of a geomembrane lined reservoir embankment," *Geotextiles and Geomembranes*, vol. 46, no. 1, pp. 52–65, 2018.

[2] H. A. Chehade, D. Dias, M. Sadek, O. Jenck, and F. H. Chehade, "Seismic analysis of geosynthetic-reinforced retaining wall in cohesive soils," *Geotextiles and Geomembranes*, vol. 47, no. 3, pp. 315–326, 2019.

[3] N. S. Correia and J. G. Zornberg, "Strain distribution along geogrid-reinforced asphalt overlays under traffic loading," *Geotextiles and Geomembranes*, vol. 46, no. 1, pp. 111–120, 2018.

[4] D. Marx and S. W. Jacobsz, "Optimal placement of reinforcement in piggyback landfill liners," *Geotextiles and Geomembranes*, vol. 46, no. 3, pp. 327–337, 2018.

[5] A. Pant, M. Datta, and G. V. Ramana, "Bottom ash as a backfill material in reinforced soil structures," *Geotextiles and Geomembranes*, vol. 47, no. 4, pp. 514–521, 2019.

[6] A. J. Puppala, P. Ruttanaporamakul, and S. S. Congress, "Design and construction of lightweight EPS geofoam embedded geomaterial embankment system for control of settlements," *Geotextiles and Geomembranes*, vol. 47, no. 3, pp. 295–305, 2019.

[7] L. A. Sanudofontaneda, S. Coupe, S. Charlesworth, and E. G. Rowlands, "Exploring the effects of geotextiles in the performance of highway filter drains," *Geotextiles and Geomembranes*, vol. 46, no. 5, pp. 559–565, 2018.

[8] Y. Yang, Z. Wei, G. Cao et al., "A case study on utilizing geotextile tubes for tailings dams construction in China," *Geotextiles and Geomembranes*, vol. 47, no. 2, pp. 187–192, 2019.

[9] G. Basu, A. N. Roy, P. Sanyal, and K. Mitra, "Bioengineering of river earth embankment using natural fibre-based

composite-structured geotextiles," *Geotextiles and Geomembranes*, vol. 47, no. 4, pp. 493–501, 2019.

[10] G. Gregory, "New materials technology in Japan," *International Journal of Materials and Product Technology*, vol. 2, no. 1, pp. 1–17, 1987.

[11] M. Mirzababaei, A. Arulrajah, S. Horpibulsuk, A. Soltani, and N. Khayat, "Stabilization of soft clay using short fibers and poly vinyl alcohol," *Geotextiles and Geomembranes*, vol. 46, no. 5, pp. 646–655, 2018.

[12] M. Prambauer, C. Wendeler, J. Weitzenbock, and C. Burgstaller, "Biodegradable geotextiles - an overview of existing and potential materials," *Geotextiles and Geomembranes*, vol. 47, no. 1, pp. 48–59, 2019.

[13] S. J. Peng, W. L. Xie, Y. Ma, and J. D. Wang, "Influence of Moisture content on strength of loess with different reinforcements," *Bulletin of Soil and Water Conservation*, vol. 33, no. 4, pp. 275–278, 2013, in Chinese.

[14] L. M. Sun, C. Y. Liu, and C. R. He, "Triaxial test study on reinforced soil at different reinforcing patterns," *Design of Hydroelectric Power Station*, vol. 21, no. 2, pp. 60–65, 2005, in Chinese.

[15] Y. Z. Wang, X. F. Liu, Z. K. Zhang, D. G. Ma, and Y. Q. Cui, "Experimental research on influence of root content on strength of undisturbed and remolded grassroots-reinforced soil," *Rock and Soil Mechanics*, vol. 8, no. 8, pp. 1405–1410, 2015, in chinese.

[16] W. L. Xie, J. D. Wang, and Y. L. Wang, "Triaxial tests study on deformation and strength characteristics of reinforced loess," *Advance in earth science*, vol. 19, no. 6, pp. 333–339, 2004, in chinese.

[17] M. X. Zhang, H. Zhou, and A. A. Javadi, "Experimental and theoretical investigation of strength of soil reinforced with multi-layer horizontal-vertical orthogonal elements," *Geotextiles and Geomembranes*, vol. 26, no. 1, pp. 1–13, 2008.

[18] M. X. Zhang, G. F. Chen, and Y. Zhu, "Triaxial tests on saturated sands reinforced with horizontal vertical inclusions," *Rock and Soil Mechanics*, vol. 31, no. 5, pp. 1345–1351, 2010, in Chinese.

[19] S. X. Chai, P. Wang, and X. Y. Wang, "Effect of reinforcing range and cross section of wheat straw on shear strength of reinforced soil," *Rock and Soil Mechanics*, vol. 34, no. 1, pp. 123–127, 2013, in Chinese.

[20] L. H. Su, N. Li, and C. H. Zhu, "Triaxial creep tests on geotextile reinforced soil[J]," *Chinese Journal of Rock Mechanics and Engineering*, vol. 35, no. 6, pp. 1273–1280, 2016, in Chinese.

[21] X. Shi, J. S. Zhang, F. Meng, S. Wang, and G. D. Deng, "Large-scale triacial test of reinforced coarse-gained soils," *Journal of Sichuan university (Enginerring Science Edition)*, vol. 46, no. 2, pp. 52–58, 2014, in Chinese.

[22] W. G. Xu, J. S. Zhang, and J. Q. He, "Resaech on large-scale triaxal test on reinforced soft rock composed of coarse-crained soil as embankment filing," *Chinese Journal of Rock Mechanics and Engineering*, vol. 29, no. 3, pp. 535–541, 2010, in Chinese.

[23] W. L. Xie, J. G. Xue, and B. Chang, "Triaxial test on dynam ic properties of reinforced soil," *Journal of catastrophology*, vol. 23, no. 1, pp. 120–124, 2008, in Chinese.

[24] Q. Z. Chen, Y. M. Liu, and S. Y. Pu, "Strength characteristics of nonpenetrating joint rock mass under different shear conditions," *Advances in Civil Engineering*, vol. 2020, Article ID 3579725, 13 pages, 2020.

[25] D. C. Feng and B. Fu, "Shear strength of internal reinforced concrete beam-column joints: intelligent modeling approach and sensitivity analysis," *Advances in Civil Engineering*, vol. 2020, Article ID 8850417, 19 pages, 2020.

[26] M. Ehrlich, M. S. Almeida, and D. Curcio, "Hydro-mechanical behavior of a lateritic fiber-soil composite as a waste containment liner," *Geotextiles and Geomembranes*, vol. 47, no. 1, pp. 42–47, 2019.

[27] J. Guo, J. Han, X. Zhang, and Z. Li, "Evaluation of moisture reduction in aggregate base by wicking geotextile using soil column tests," *Geotextiles and Geomembranes*, vol. 47, no. 3, pp. 306–314, 2019.

[28] E. M. Palmeira, D. L. Melo, and I. P. Moraesfilho, "Geotextile filtration opening size under tension and confinement," *Geotextiles and Geomembranes*, vol. 47, no. 4, pp. 566–576, 2019.

[29] G. Stoltz, P. Delmas, and C. Barral, "Comparison of the behaviour of various geotextiles used in the filtration of clayey sludge: an experimental study," *Geotextiles and Geomembranes*, vol. 47, no. 2, pp. 230–242, 2019.

[30] K. Sweta and S. K. Hussaini, "Behavior evaluation of geogrid-reinforced ballast-subballast interface under shear condition," *Geotextiles and Geomembranes*, vol. 47, no. 1, pp. 23–31, 2019.

[31] H. Chen, X. Liu, S. Feng, and J. Chen, "A. Microscale investigation into mechanical behaviors of heat-bonded nonwoven geotextile using DEM," *Geotextiles and Geomembranes*, vol. 47, no. 3, pp. 429–438, 2019.

[32] X. Cui, Y. Wang, K. Liu et al., "A simplified model for evaluating the hardening behaviour of sensor-enabled geobelts during pullout tests," *Geotextiles and Geomembranes*, vol. 47, no. 3, pp. 377–388, 2019.

[33] J. O. Neto, "Application of the two-layer system theory to calculate the settlements and vertical stress propagation in soil reinforcement with geocell," *Geotextiles and Geomembranes*, vol. 47, no. 1, pp. 32–41, 2019.

[34] Y. Wang, Z. H. Hu, Y. H. Chen, and H. T. Xiao, "Two-dimensional parametric study of an embankment on clay improved by an artificial crust composite foundation," *Advances in Civil Engineering*, vol. 2020, Article ID 8858380, 16 pages, 2020.

[35] X. M. Jiang, H. S. Niu, W. P. Huang, X. W. Shang, and D. Wang, "Experimental study on noncoaxial characteristics of saturated remolded loess," *Advances in Civil Engineering*, vol. 2020, Article ID 8872356, 10 pages, 2020.

[36] F. Zhang, D. Leshchinsky, Y. Gao, and S. Yang, "Corner reinforced slopes: required strength and length of reinforcement based on internal stability," *Geotextiles and Geomembranes*, vol. 47, no. 3, pp. 408–416, 2019a.

[37] L. Zhao, W. Zhou, X. Geng, K. Yuen, and B. Fatahi, "A closed-form solution for column-supported embankments with geosynthetic reinforcement," *Geotextiles and Geomembranes*, vol. 47, no. 3, pp. 389–401, 2019.

[38] M. J. I. Alam, C. T. Gnanendran, and S. R. Lo, "Experimental and numerical investigations of the behaviour of footing on geosynthetic reinforced fill slope under cyclic loading," *Geotextiles and Geomembranes*, vol. 46, no. 6, pp. 848–859, 2018a.

[39] A. Ouria and A. Mahmoudi, "Laboratory and numerical modeling of strip footing on geotextile-reinforced sand with cement-treated interface," *Geotextiles and Geomembranes*, vol. 46, no. 1, pp. 29–39, 2018.

[40] P. Colajanni, M. Papia, and M. Spinella, "Stress-strain law for confined concrete with hardening or softening behavior," *Advances in Civil Engineering*, vol. 2013, Article ID 804904, 11 pages, 2013.

[41] A. Skejic, S. Medic, and S. Dolarevic, "Influence of wire mesh characteristics on reinforced soil model wall failure mechanisms-physical and numerical modelling," *Geotextiles and Geomembranes*, vol. 46, no. 6, pp. 726–738, 2018.

[42] F. Song, H. Liu, L. Ma, and H. Hu, "Numerical analysis of geocell-reinforced retaining wall failure modes," *Geotextiles and Geomembranes*, vol. 46, no. 3, pp. 284–296, 2018.

[43] D. Stevanovic, S. Kalyanasundaram, A. Lowe, and P. Y. Jar, "Numerical simulation of elastic-plastic interlaminar crack propagation in interlayer-toughened composite materials," *International Journal of Materials and Product Technology*, vol. 17, no. 1-2, pp. 99–107, 2002.

[44] X. G. Liu, W. C. Zhu, and L. K. Li, "Numerical shear tests on the scale effect of rock joints under CNL and CND conditions," *Advances in Civil Engineering*, vol. 2020, Article ID 6465231, 15 pages, 2020.

[45] J. Zhang, M. Zhang, P. Zhai, L. Liu, and H. Shi, "Numerical simulation on the impact resistance of functionally graded materials," *International Journal of Materials and Product Technology*, vol. 42, no. 1-2, pp. 87–97, 2011.

[46] Y. Zheng, P. J. Fox, and J. S. Mccartney, "Numerical study on maximum reinforcement tensile forces in geosynthetic reinforced soil bridge abutments," *Geotextiles and Geomembranes*, vol. 46, no. 5, pp. 634–645, 2018.

[47] Z. Zhang, M. Wang, G. Ye, and J. Han, "A novel 2D-3D conversion method for calculating maximum strain of geosynthetic reinforcement in pile-supported embankments," *Geotextiles and Geomembranes*, vol. 47, no. 3, pp. 336–351, 2019b.

[48] P. Shen, J. Han, J. G. Zornberg et al., "Two and three-dimensional numerical analyses of geosynthetic-reinforced soil (GRS) piers," *Geotextiles and Geomembranes*, vol. 47, no. 3, pp. 352–368, 2019.

[49] Y. Chen, Y. Gao, S. Yang, and F. Zhang, "Required unfactored geosynthetic strength of three-dimensional reinforced soil structures comprised of cohesive backfills," *Geotextiles and Geomembranes*, vol. 46, no. 6, pp. 860–868, 2018.

[50] G. Gao and M. A. Meguid, "Effect of particle shape on the response of geogrid-reinforced systems: insights from 3D discrete element analysis," *Geotextiles and Geomembranes*, vol. 46, no. 6, pp. 685–698, 2018.

[51] S. T. Kadhim, R. L. Parsons, and J. Han, "Three-dimensional numerical analysis of individual geotextile-encased sand columns with surrounding loose sand," *Geotextiles and Geomembranes*, vol. 46, no. 6, pp. 836–847, 2018.

[52] J. G. Zhu, R. R. Shakir, Y. L. Yang, and K. Peng, "Comparison of behaviors of soil-concrete interface from ring-shear and simple shear tests," *Rock and Soil Mechanics*, vol. 32, no. 3, pp. 692–696, 2011, in Chinese.

[53] R. P. Hillman and T. D. Stark, "Shear strength characteristics of PVC geomembrane-geosynthetic interfaces," *Geosynthetics International*, vol. 8, no. 2, pp. 135–162, 2001.

[54] Y. Ong, T. Sun, and M. T. Luan, "Development and application of geotechnical ring shear apparatus: anoverview," *Rock and Soil Mechanics*, vol. 30, no. 3, pp. 628–634, 2009, in Chinese.

[55] Y. L. Yang, J. G. Zhu, and T. Yu, "Experimental study on mechanical behaviour of soil-structure interface by ring shear test," *Rock and Soil Mechanics*, vol. 30, no. 11, pp. 3256–3260, 2009, in Chinese.

[56] A. K. Choudhary, B. Pandit, and G. L. Babu, "Uplift capacity of horizontal anchor plate in geocell reinforced sand," *Geotextiles and Geomembranes*, vol. 47, no. 2, pp. 203–216, 2019.

[57] S. Goodarzi and H. Shahnazari, "Strength enhancement of geotextile-reinforced carbonate sand," *Geotextiles and Geomembranes*, vol. 47, no. 2, pp. 128–139, 2019.

[58] J. Wang, L. Zhang, J. Xue, and Y. Tang, "Load-settlement response of shallow square footings on geogrid-reinforced sand under cyclic loading," *Geotextiles and Geomembranes*, vol. 46, no. 5, pp. 586–596, 2018.

[59] C. Xu, C. Liang, and P. Shen, "Experimental and theoretical studies on the ultimate bearing capacity of geogrid-reinforced sand," *Geotextiles and Geomembranes*, vol. 47, no. 3, pp. 417–428, 2019.

[60] P. J. R. De Albuquerque and D. R. Leon-Mogrovejo, "A laboratory investigation on a mechanical behavior of sandy and clayey soils with kraft paper fiber," *Transp Infrastruct G*, vol. 8, no. 1, pp. 12–36, 2021.

[61] G. H. Wang and K. Sassa, "Post-failure mobility of saturated sands in undrained load-controlled ring shear tests," *Canadian Geotechnical Journal*, vol. 39, no. 4, pp. 821–837, 2002.

[62] F. Y. Zhang and G. H. Wang, "Effect of irrigation-induced densification on the post-failure behavior of loess flowslides occurring on the Heifangtai area, Gansu, China," *Engineering Geology*, vol. 236, pp. 111–118, 2018.

[63] F. Y. Zhang, G. H. Wang, K. Toshitaka, W. W. Chen, D. X. Zhang, and J. Yang, "Undrained shear behavior of loess saturated with different concentrations of sodium chloride solution," *Engineering Geology*, vol. 155, pp. 69–79, 2013.

[64] Q. Y. Guo, T. F. Gu, and Y. Z. U, "A test study of unsaturated loess in Yongjing County," *Hydrogeology & Engineering Geology*, vol. 42, no. 6, pp. 103–113, 2015, in Chinese.